



Cite this: DOI: 10.1039/c6dt02953a

# Effect of the S-to-S bridge on the redox properties and H<sub>2</sub> activation performance of diiron complexes related to the [FeFe]-hydrogenase active site†

Minglun Cheng,<sup>a</sup> Mei Wang,<sup>\*a</sup> Dehua Zheng<sup>a</sup> and Licheng Sun<sup>a,b</sup>

Three biomimetic models of the [FeFe]-hydrogenase active site, namely diiron dithiolates of [(μ-edt){Fe(CO)<sub>3</sub>}{Fe(CO)(κ<sup>2</sup>-PNP)}] (**1**, edt = ethane-1,2-dithiolate, PNP = Ph<sub>2</sub>PCH<sub>2</sub>N(*n*Pr)CH<sub>2</sub>PPh<sub>2</sub>), [(μ-bdtMe){Fe(CO)<sub>3</sub>}{Fe(CO)(κ<sup>2</sup>-PNP)}] (**2**, bdtMe = 4-methylbenzene-1,2-dithiolate), and [(μ-adtBn){Fe(CO)<sub>3</sub>}{Fe(CO)(κ<sup>2</sup>-PNP)}] (**3**, adtBn = *N*-benzyl-2-azapropane-1,3-dithiolate), were prepared and structurally characterized. These complexes feature the same PNP ligand but different S-to-S bridges. Influence of the S-to-S bridge on the electrochemical properties and chemical oxidation reactivity of **1–3** was studied by cyclic voltammetry and by *in situ* IR spectroscopy. The results reveal that the S-to-S bridge has a considerable effect on the oxidation reactivity of **1–3** and on the stability of *in situ* generated single-electron oxidized complexes, [**1**]<sup>+</sup>, [**2**]<sup>+</sup>, and [**3**]<sup>+</sup>. The performances of [**1**]<sup>+</sup> and [**2**]<sup>+</sup> for H<sub>2</sub> activation were explored in the presence of a mild chemical oxidant, while rapid decomposition of [**3**]<sup>+</sup> thwarted the further study of this complex. Gratifyingly, **1** was found to be catalytically active, although in a low turnover number, for H<sub>2</sub> oxidation in the presence of excess mild oxidant and a proton trapper under 1 atm H<sub>2</sub> at room temperature.

Received 26th July 2016,  
Accepted 4th October 2016  
DOI: 10.1039/c6dt02953a

www.rsc.org/dalton

## Introduction

[FeFe]-hydrogenase ([FeFe]-H<sub>2</sub>ase) enzymes are a kind of metalloenzymes which reversibly catalyze the redox of H<sub>2</sub>/H<sup>+</sup> at remarkable reaction rates.<sup>1–4</sup> At the end of the last century, the structure of [FeFe]-H<sub>2</sub>ases was elucidated by high-resolution X-ray crystallography.<sup>5,6</sup> Subsequent theoretical and spectroscopic studies suggest that the [FeFe]-H<sub>2</sub>ases exist in different redox states, namely the super reduced state (H<sub>sred</sub>),<sup>7</sup> the reduced state (H<sub>red</sub>), the oxidized active state (H<sub>ox</sub>), the CO-inhibited state (H<sub>ox</sub><sup>CO</sup>),<sup>8</sup> and the oxidized inactive state (H<sub>ox</sub><sup>air</sup>).<sup>9,10</sup> Among them, H<sub>red</sub> and H<sub>ox</sub> states (Fig. 1) have drawn extensive attention as the former is believed to be an active state for H<sub>2</sub> formation and the latter to be an active state for H<sub>2</sub> uptake.

<sup>a</sup>State Key Laboratory of Fine Chemicals, DUT-KTH Joint Education and Research Center on Molecular Devices, Dalian University of Technology, Dalian 116024, China. E-mail: symbueno@dlut.edu.cn

<sup>b</sup>Department of Chemistry, KTH Royal Institute of Technology, Stockholm, 10044, Sweden

† Electronic supplementary information (ESI) available: Selected bond lengths (Å) and angles (°) for **1–3** and **2'** (Table S1), crystal data and structural refinements details for **1–3** and **2'** (Table S2), molecular structure of **2'** (Fig. S1), IR and <sup>31</sup>P NMR spectra (Fig. S2–S7), and additional CV of **1** (Fig. S8). CCDC 1495096–1495099. For ESI and crystallographic data in CIF or other electronic format see DOI: 10.1039/C6DT02953A

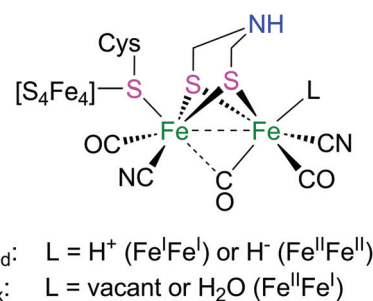


Fig. 1 H<sub>red</sub> and H<sub>ox</sub> states of the [FeFe]-H<sub>2</sub>ase active site.

Over the past decade, studies on the mimicking of [FeFe]-H<sub>2</sub>ases have been carried out mostly on the H<sub>red</sub> models and their electrochemical and photochemical proton reduction performances,<sup>11–17</sup> while less attention has been paid to mimic the H<sub>ox</sub> state and the H<sub>2</sub> oxidation reaction.<sup>18–23</sup> To date, only a few mixed-valence H<sub>ox</sub> models were found to be capable of activating H<sub>2</sub> under mild conditions. The pioneering work by Rauchfuss and co-workers revealed that the mixed-valence complexes, [(μ-adtBn){Fe(CO)<sub>2</sub>(PMe<sub>3</sub>)}{Fe(CO)(κ<sup>2</sup>-dppv)}]<sup>+</sup> (adtBn = *N*-benzyl-2-azapropane-1,3-dithiolate, dppv = *cis*-1,2-bis-(diphenylphosphino)ethene) and [(μ-adtBn){Fe(CO)<sub>3</sub>}{Fe(CO)(κ<sup>2</sup>-dppn)}]<sup>+</sup> (dppn = 1,8-bis(diphenylphos-

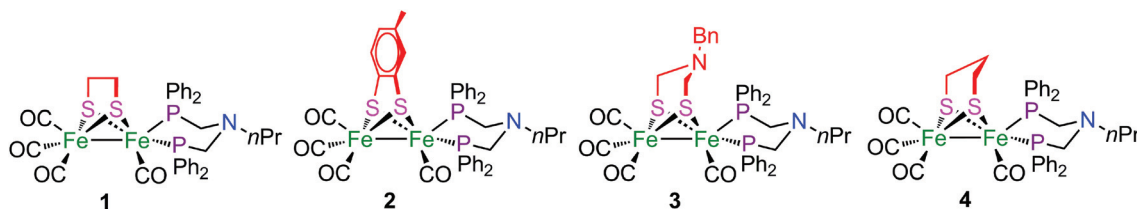


Fig. 2 Structures of the [FeFe]-H<sub>2</sub>ase mimics 1–4.

phino)naphthalene), reacted with 1 atm H<sub>2</sub> at 20 °C in the presence of FcBAR<sup>F</sup><sub>4</sub> (Fc<sup>+</sup> = [FeCp<sub>2</sub>]<sup>+</sup>, Cp = C<sub>5</sub>H<sub>5</sub>; BAR<sup>F</sup><sub>4</sub><sup>−</sup> = B(3,5-C<sub>6</sub>H<sub>3</sub>(CF<sub>3</sub>)<sub>2</sub>)<sub>4</sub><sup>−</sup>) to generate intermediates containing both a μ-hydride at the diiron center and a proton at the pendant N atom.<sup>24,25</sup> Subsequently, a diiron azadithiolate model, [(μ-adtBn){Fe(CO)<sub>2</sub>(FcP\*)}{Fe(CO)(κ<sup>2</sup>-dppv)}] (FcP\* = Cp\*Fe(C<sub>5</sub>Me<sub>4</sub>CH<sub>2</sub>PEt<sub>2</sub>), Cp\* = C<sub>5</sub>Me<sub>5</sub>), was designed by the same group with FcP\* as a one-electron redox module to mimic the redox function of an Fe<sub>4</sub>S<sub>4</sub> cluster in the [FeFe]-H<sub>2</sub>ases, which gave the first example for the catalytic oxidation of 1 atm H<sub>2</sub> by a model of [FeFe]-H<sub>2</sub>ases in the presence of excess oxidant (FcBAR<sup>F</sup><sub>4</sub>) and a proton trapper (P(*o*-tol)<sub>3</sub>) at room temperature.<sup>26</sup> Except for this special example, the previously reported H<sub>ox</sub> models with a built-in amine in the center of the S-to-S bridge activated H<sub>2</sub> only stoichiometrically under 1 atm H<sub>2</sub> in the presence of a mild oxidant and a proton trapper, because the stable μ-hydride intermediates formed in the reaction processes cannot be deprotonated by a weak base to recover the starting neutral diiron complexes and therefore cannot finish the catalytic cycle.

In our previous work, we found that the μ-hydride in the diiron dithiolate complexes with a built-in amine in the center of an unsymmetrically chelating diphosphine ligand, Ph<sub>2</sub>PCH<sub>2</sub>N(*n*Pr)CH<sub>2</sub>PPh<sub>2</sub> (PNP), could be readily deprotonated in the presence of a weak base.<sup>27,28</sup> The DFT calculation suggests that the deprotonation of the PNP-coordinating diiron μ-hydride complex takes place *via* an indirect pathway, in which the accessible pendant amine of the PNP ligand acts as a proton shuttle so as to lower the energy barriers for the deprotonation of diiron μ-hydride complexes.<sup>29</sup> Moreover, we found that complex [(μ-pdt){Fe(CO)<sub>3</sub>}{Fe(CO)(κ<sup>2</sup>-PNP)}] (pdt = propane-1,3-dithiolate) catalytically activated H<sub>2</sub> under 1 atm H<sub>2</sub> at 25 °C in the presence of excess Fc<sup>+</sup> and P(*o*-tol)<sub>3</sub>.<sup>30</sup> One of the general questions arising from the study on this type of Fe<sub>2</sub>S<sub>2</sub> complexes concerns the influence of the S-to-S bridge on the structure and reactivity of the underlying Fe<sub>2</sub>(CO)<sub>6-x</sub>L<sub>x</sub> subunit. A better understanding of how the S-to-S bridge affects the redox properties, stability and reactivity of the underlying diiron centers will be helpful for the reasonable design of new H<sub>ox</sub> models for H<sub>2</sub> activation.

In this context, we tried to find the influence of the S-to-S bridge on the redox properties and H<sub>2</sub>-uptake capability of the H<sub>ox</sub> models bearing a PNP ligand. Here we report the preparation and molecular structures of three new Fe<sub>2</sub>S<sub>2</sub> complexes, [(μ-edt){Fe(CO)<sub>3</sub>}{Fe(CO)(κ<sup>2</sup>-PNP)}] (**1**, edt = ethane-1,2-dithiolate), [(μ-bdtMe){Fe(CO)<sub>3</sub>}{Fe(CO)(κ<sup>2</sup>-PNP)}] (**2**, bdtMe =

4-methylbenzene-1,2-dithiolate), and [(μ-adtBn){Fe(CO)<sub>3</sub>}{Fe(CO)(κ<sup>2</sup>-PNP)}] (**3**). These complexes, together with the previously reported analogous diiron complex [(μ-pdt){Fe(CO)<sub>3</sub>}{Fe(CO)(κ<sup>2</sup>-PNP)}] (**4**, pdt = propane-1,3-dithiolate), feature the same pendant amine-containing diphosphine ligand, but have different S-to-S bridges (Fig. 2). The influence of the S-to-S bridge on the electrochemical properties and chemical oxidation reactivity of **1–3** and on the stability of their corresponding Fe<sup>II</sup>Fe<sup>I</sup> mixed-valence complexes was studied by cyclic voltammetry and *in situ* IR spectroscopy. Among the H<sub>ox</sub> models of [**1**]<sup>+</sup>–[**4**]<sup>+</sup>, [**1**]<sup>+</sup> and [**4**]<sup>+</sup> were catalytically active for H<sub>2</sub> oxidation in the presence of FcBAR<sup>F</sup><sub>4</sub> and P(*o*-tol)<sub>3</sub> under mild conditions, whereas [**2**]<sup>+</sup> was decomposed to a mononuclear iron complex [Fe(CO)(κ<sup>2</sup>-bdtMe)(κ<sup>2</sup>-PNP)] (**2'**) under the same reaction conditions. Complex **2'** was readily oxidized to an Fe<sup>III</sup> species (**2''**) in the presence of FcBAR<sup>F</sup><sub>4</sub>. Unfortunately, the poor stability of [**3**]<sup>+</sup> thwarted the study on [**3**]<sup>+</sup> for the H<sub>2</sub> activation reaction.

## Results and discussion

### Preparation and characterization of 1–3

Complexes **1–3** were prepared from the reaction of [(μ-edt)Fe<sub>2</sub>(CO)<sub>3</sub>], [(μ-bdtMe)Fe<sub>2</sub>(CO)<sub>6</sub>], and [(μ-adtBn)Fe<sub>2</sub>(CO)<sub>6</sub>] with the PNP ligand, respectively, in refluxing toluene for 3 h. Analytically pure complexes of **1–3** were obtained by chromatography and recrystallization of the crude products. The products were characterized by ESI-HRMS (electrospray ionization high resolution mass spectroscopy), IR, <sup>1</sup>H and <sup>31</sup>P{<sup>1</sup>H} NMR spectroscopy. The HRMS data of the products are in good agreement with the proposed compositions of **1–3**. The <sup>1</sup>H and <sup>31</sup>P{<sup>1</sup>H} NMR spectra confirm that complexes **1–3** have similar structures, in which one of the iron centers is chelated by the PNP ligand. The IR data of the ν<sub>CO</sub> absorptions of **1–3** are summarized in Table 1, together with the ν<sub>CO</sub> absorptions of the

Table 1 Comparison of ν<sub>CO</sub> absorptions of the related Fe<sup>I</sup>Fe<sup>I</sup> and Fe<sup>II</sup>Fe<sup>I</sup> complexes

Complex	ν <sub>CO</sub> (cm <sup>-1</sup> ), n = 0 (Fe <sup>I</sup> Fe <sup>I</sup> )	ν <sub>CO</sub> (cm <sup>-1</sup> ), n = +1 (Fe <sup>II</sup> Fe <sup>I</sup> )	Ref.
[ <b>1</b> ] <sup>n</sup>	2028, 1956, 1900	2088, 2031, 1901	This work
[ <b>2</b> ] <sup>n</sup>	2033, 1963, 1901	2090, 2036, 1911	This work
[ <b>3</b> ] <sup>n</sup>	2026, 1955, 1901	2086, 2027, 1908	This work
[ <b>4</b> ] <sup>n</sup>	2025, 1953, 1898	2081, 2022, 1900	27

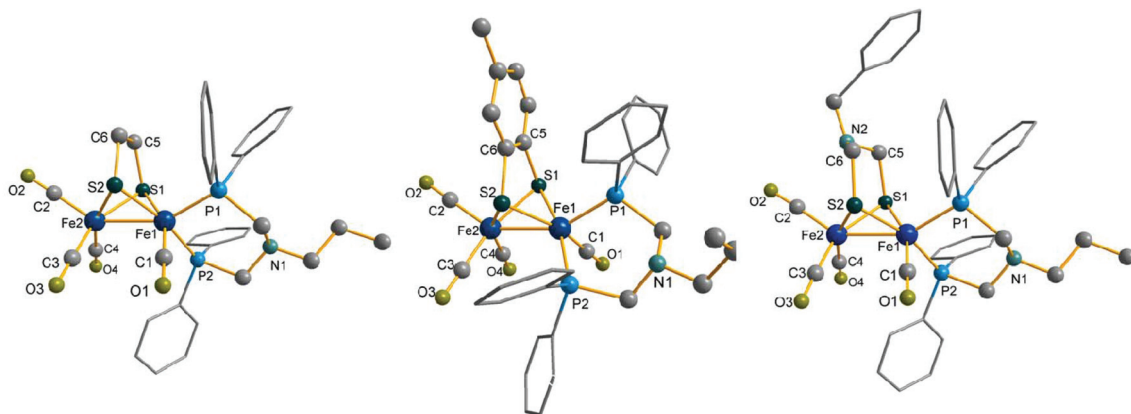


Fig. 3 Molecule structures of **1** (left), **2** (middle) and **3** (right) as ball and stick drawings. Hydrogen atoms are omitted for clarity.

analogous complex **4**.<sup>27,28</sup> These diiron complexes each contain four carbonyl ligands and an unsymmetrically bidentate diphosphine ligand. In the IR spectra, the  $\nu_{\text{CO}}$  absorption of the lowest wavenumber around  $1900\text{ cm}^{-1}$  is attributed to the vibration of the CO ligand in the  $\text{Fe}(\text{CO})(\text{PNP})$  unit. The other two  $\nu_{\text{CO}}$  absorptions at higher wavenumbers are assigned to the vibrations of CO ligands in the  $\text{Fe}(\text{CO})_3$  unit. In general, the  $\nu_{\text{CO}}$  bands of **1–4** display a tendency to blue shift as the S-to-S bridge is changed from pdt to adtBn, edt, and then to bdtMe, indicating that the change of the S-to-S bridge can finely tune the electron back-bonding from the iron center to the anti-bonding  $\pi^*$ -orbital of the coordinated CO. Among these diiron complexes, **2** exhibits the apparently higher wavenumbers for the  $\nu_{\text{CO}}$  absorptions of the  $\text{Fe}(\text{CO})_3$  unit due to the electron-withdrawing character of the aromatic bdt-bridge.

The molecular structures of **1–3** were determined by single crystal X-ray diffraction analyses, which are shown in Fig. 3 as ball and stick drawings. Selected bond lengths and angles for **1–3** are listed in Table S1.† The  $\text{Fe}_2\text{S}_2$  cores of these complexes have a butterfly framework and each iron atom is coordinated in a pseudo-square pyramidal geometry as in other biomimetic diiron dithiolate complexes.<sup>31–33</sup> In the solid state, the chelating PNP ligand lies in an apical/basal configuration at the Fe1 atom of each complex, being analogous to the previously reported PNP-coordinating diiron dithiolate complex with a pdt bridge.<sup>28</sup> The Fe–Fe bond distances are in the order of **2** ( $2.5429(6)\text{ \AA}$ ) < **1** ( $2.5618(7)\text{ \AA}$ ) < **3** ( $2.5825(10)\text{ \AA}$ ), indicating that the stronger rigidity of the S-to-S bridge leads to a shorter Fe–Fe bond. It is worth noting that the Fe2–S bonds are  $0.013\text{--}0.015\text{ \AA}$  longer than the Fe1–S bonds in the same complex, and the Fe2–S bonds ( $2.2654\text{--}2.2875\text{ \AA}$ ) in **2** and **3** are observably longer than those ( $2.2582\text{--}2.2639\text{ \AA}$ ) in **1**. The subtle difference in the Fe–S bond lengths may influence the stability of the  $\text{Fe}_2\text{S}_2$  core during the oxidation process, which will be discussed in the following section.

### Electrochemical properties of **1–4**

To explore the influence of the S-to-S bridge in the second coordination sphere on the redox properties of PNP-coordinat-

ing diiron complexes, the electrochemistry of **1–4** was studied by cyclic voltammetry in  $\text{CH}_2\text{Cl}_2$ . Complex **1** displayed a reversible oxidation event at  $E_{1/2}^{\text{ox1}} = -0.11\text{ V}$  (all potentials given in this paper are *versus*  $\text{Fc}^{+/0}$  potential.) with a peak potential  $E_p^{\text{ox1}} = -0.05\text{ V}$  for the  $\text{Fe}^{\text{I}}\text{Fe}^{\text{I}}/\text{Fe}^{\text{II}}\text{Fe}^{\text{I}}$  couple and an irreversible oxidation peak at  $E_p^{\text{ox2}} = +0.85\text{ V}$  for the  $\text{Fe}^{\text{II}}\text{Fe}^{\text{I}}/\text{Fe}^{\text{II}}\text{Fe}^{\text{II}}$  process (Fig. 4a), which are similar to the corresponding oxidation events of **4** (Fig. 4d). It is noted that in addition to the reduction events for  $[\mathbf{1}]^{2+}/[\mathbf{1}]^+$  at about  $+0.68\text{ V}$  and for  $[\mathbf{1}]^+/1$  at  $-0.18\text{ V}$ , an extra small reduction peak appears at  $-0.51\text{ V}$  in the second run of cyclic voltammetry (CV), which is not observed in the first run scanning in the cathodic direction. When the anodic scan returns before  $+0.65\text{ V}$  to avoid the second oxidation process, the reduction peak at  $-0.51\text{ V}$  does not appear in the subsequent cathodic scan. These observations indicate that the reduction event at  $-0.51\text{ V}$  is the reduction of the decomposed product of the second oxidation process and the structure of this product is currently not clear. Noticeably, such an extra weak-intensity reductive event also appears in the CV of **4** but not observed in the CVs of **2** and **3**. The potential of the first oxidation event ( $E_{1/2}^{\text{ox1}}$ ) of **2** (Fig. 4b) is almost identical to the  $[\mathbf{1}]^+/1$  couple, while the second irreversible oxidation peak ( $E_p^{\text{ox2}} = +0.60\text{ V}$ ) of **2** is  $270\text{ mV}$  less positive than the  $[\mathbf{1}]^{2+}/[\mathbf{1}]^+$  couple. The CV of **3** shows a quasi-reversible oxidation event at  $E_{1/2}^{\text{ox1}} = -0.20\text{ V}$  ( $E_p^{\text{ox1}} = -0.08\text{ V}$ ) and an irreversible peak at  $E_p^{\text{ox2}} = +0.42\text{ V}$  for the further  $\text{Fe}^{\text{II}}\text{Fe}^{\text{I}}$  to  $\text{Fe}^{\text{II}}\text{Fe}^{\text{II}}$  oxidation process (Fig. 4c).

Table 2 summarizes the oxidation potentials of **1–4**,<sup>30</sup> together with those of  $[\text{Fe}_2(\mu\text{-edt})(\text{CO})_3(\kappa^2\text{-dppv})(\text{PMe}_3)]$  (**5**),<sup>34</sup>  $[\text{Fe}_2(\mu\text{-pdt})(\text{CO})_3(\kappa^2\text{-dppv})(\text{PMe}_3)]$  (**6**), and  $[\text{Fe}_2(\mu\text{-adtBn})(\text{CO})_3(\kappa^2\text{-dppv})(\text{PMe}_3)]$  (**7**), to gain an insight into the influence of the S-to-S linker on the electrochemical redox properties of  $[\text{FeFe}]$ -H<sub>2</sub>ase models. The comparison of the oxidation potentials for the two series of diiron complexes (**1–4** and **5–7**) provides us some interesting hints. The oxidation potential related to the  $\text{Fe}^{\text{I}}\text{Fe}^{\text{I}}/\text{Fe}^{\text{II}}\text{Fe}^{\text{I}}$  couple is not very susceptible to the electronic properties of the S-to-S bridge, especially when the bridges have the same number of atoms, while when the S-to-S bridge is shortened from 3 to 2 atoms a  $110\text{--}140\text{ mV}$  positive shift of

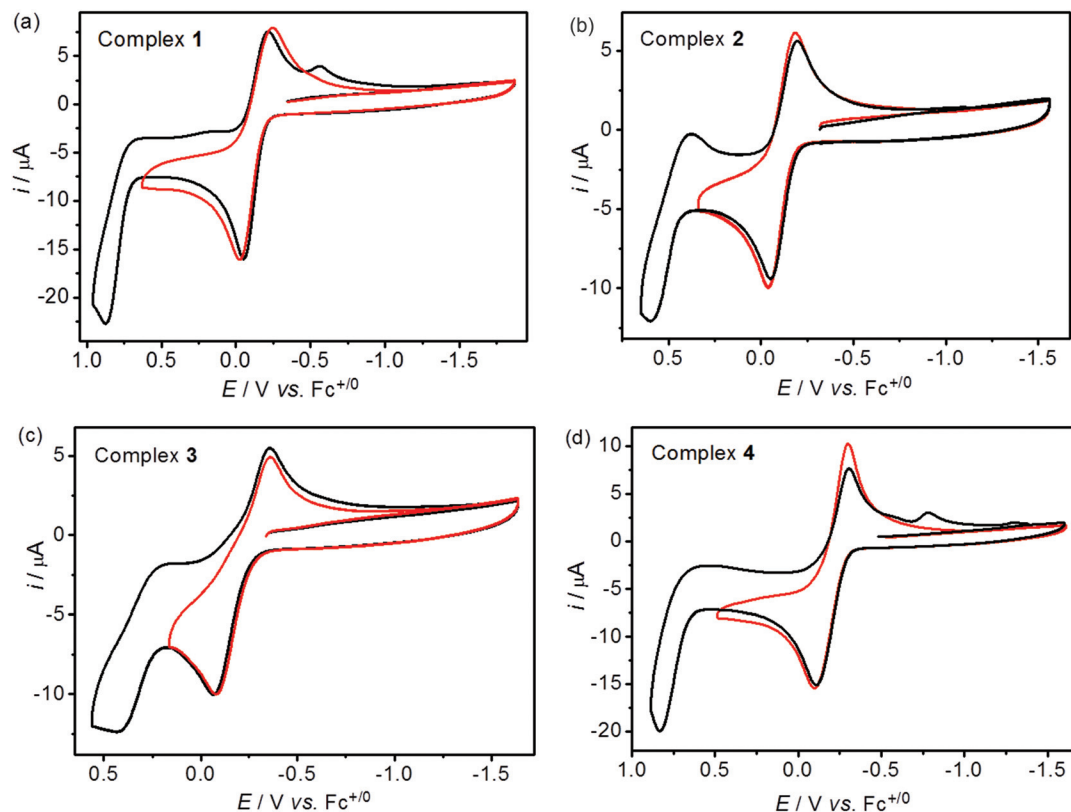


Fig. 4 Cyclic voltammograms of (a) 1, (b) 2, (c) 3, and (d) 4 (1.0 mM) with full scan (black lines) and with anodic scan returned before the onset of the second oxidation event (red lines) in 0.1 M  $n\text{Bu}_4\text{NPF}_6/\text{CH}_2\text{Cl}_2$  at a scan rate of  $100 \text{ mV s}^{-1}$ .

Table 2 Redox potentials (V vs.  $\text{Fc}^{+/0}$ ) of 1–4 and some related diiron complexes in  $n\text{Bu}_4\text{NPF}_6/\text{CH}_2\text{Cl}_2$

Complex	$E_{1/2}^{\text{ox1}}$ (V)	$E_{\text{p}}^{\text{ox1}}$ (V)	$E_{\text{p}}^{\text{ox2}}$ (V)	$\Delta E^{\text{ox} a}$ (V)	Ref.
1 (edt, PNP)	-0.11	-0.05	+0.85	0.90	This work
2 (bdtMe, PNP)	-0.10	-0.04	+0.60	0.64	This work
3 (adtBn, PNP)	-0.20	-0.09	+0.42	0.51	This work
4 (pdt, PNP)	-0.22	-0.12	+0.80	0.93	30
5 (edt, dppv, $\text{PMe}_3$ )	-0.47	-0.41	+0.42	0.83	34
6 (pdt, dppv, $\text{PMe}_3$ )	-0.61	-0.54	+0.43	0.97	34
7 (adtBn, dppv, $\text{PMe}_3$ )	-0.64	-0.58	-0.06	0.52	34

$$^a \Delta E^{\text{ox}} = |E_{\text{p}}^{\text{ox2}} - E_{\text{p}}^{\text{ox1}}|.$$

the first oxidation potential is observed for both series. In contrast, the potential corresponding to the further oxidation of  $\text{Fe}^{\text{II}}\text{Fe}^{\text{I}}$  to  $\text{Fe}^{\text{II}}\text{Fe}^{\text{II}}$  is highly dependent on the electronic properties of the S-to-S bridge but not very susceptible to the length of the S-to-S bridge. It is worth noting that the second oxidation potentials of the adt-bridging  $\text{Fe}_2\text{S}_2$  complexes are considerably less positive than those of their corresponding  $\text{Fe}_2\text{S}_2$  complexes bearing a pdt bridge, e.g.  $E_{\text{p}}^{\text{ox2}} = +0.42 \text{ V}$  for 3 (adtBn) versus  $+0.80 \text{ V}$  for 4 (pdt) and  $-0.06 \text{ V}$  for 7 (adtBn) versus  $+0.43 \text{ V}$  for 6 (pdt). Such an apparent influence of the adt bridge on the  $\text{Fe}^{\text{II}}\text{Fe}^{\text{I}}/\text{Fe}^{\text{II}}\text{Fe}^{\text{II}}$  oxidation potential is most possibly due to the coordinative interaction of the iron center and the pendant amine of the adt bridge as verified in the case of 7.<sup>34</sup>

$\Delta E^{\text{ox}}$  ( $\Delta E^{\text{ox}} = |E_{\text{p}}^{\text{ox2}} - E_{\text{p}}^{\text{ox1}}|$ ) is a significant electrochemical datum that will directly influence the  $\text{H}_2$  activation performance of  $\text{Fe}_2\text{S}_2$  complexes. Regardless of the number and the type of phosphine ligands, complexes bearing an edt and a pdt bridge display large  $\Delta E^{\text{ox}}$  values (0.83–0.97 V), which prevent the overlap of the two oxidation steps and guarantee the clean formation of the one-electron oxidized intermediate under controlled oxidation reaction. Furthermore, the chemical reversibility of the first oxidation process evinced by the current ratio,  $i_{\text{pa}}/i_{\text{pc}}$  ( $i_{\text{pa}}$  = anodic peak current,  $i_{\text{pc}}$  = cathodic peak current), is about 0.96, 0.88, 0.78, and 1 for 1–4, respectively, indicating that the S-to-S bridge does have a considerable effect on the stability of these  $[\text{FeFe}]\text{-H}_2\text{ase}$  models and their oxidized derivatives.

### Chemical oxidation of 1–3

Chemical oxidation reactions of 1–3 in  $\text{CH}_2\text{Cl}_2$  were monitored by *in situ* IR spectroscopy under  $\text{N}_2$  at room temperature using  $\text{FcBAR}^{\text{F}_4}$  as an oxidant. Upon addition of 1 equiv. of  $\text{FcBAR}^{\text{F}_4}$  to the solution of 1, the  $\nu_{\text{CO}}$  absorptions of 1 at 2028, 1956, and  $1900 \text{ cm}^{-1}$  decreased rapidly (Fig. 5a), accompanied by the appearance of a new  $\nu_{\text{CO}}$  band at  $2088 \text{ cm}^{-1}$ , while two other new  $\nu_{\text{CO}}$  bands at 2031 and  $1901 \text{ cm}^{-1}$  happened to overlap with the  $\nu_{\text{CO}}$  absorptions of 1. Therefore the  $\nu_{\text{CO}}$  band of 1 at  $1956 \text{ cm}^{-1}$  was used as an indicator of the reaction extent. The total disappearance of this band within 2 min suggests a rapid

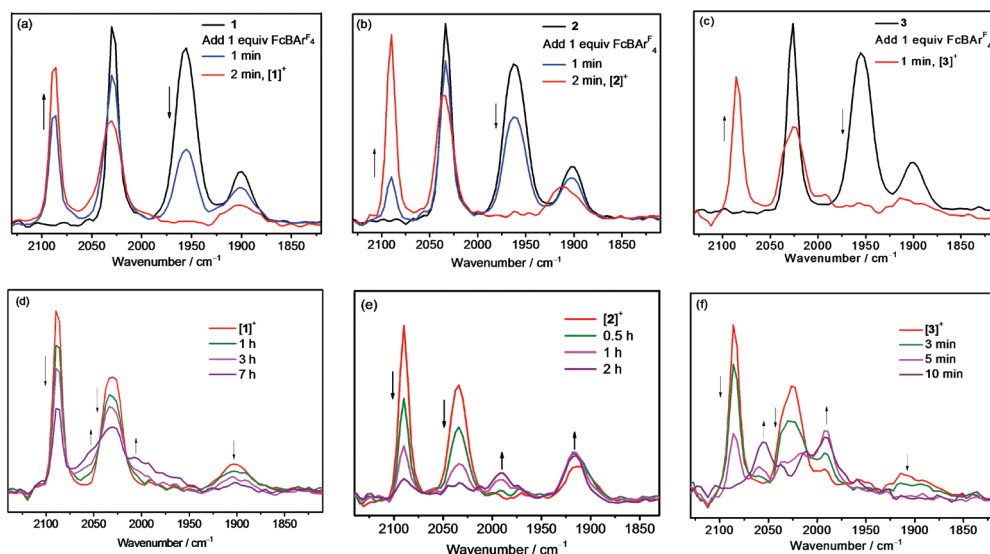


**Fig. 5** Changes of  $\nu_{\text{CO}}$  absorptions in the *in situ* IR spectra of **1** (a), **2** (b), and **3** (c) in  $\text{CH}_2\text{Cl}_2$  with the addition of an equiv. of  $\text{FcBAR}_4^{\text{F}}$ , and of the *in situ* generated  $[1]^+$  (d),  $[2]^+$  (e), and  $[3]^+$  (f) in  $\text{CH}_2\text{Cl}_2$ , standing under  $\text{N}_2$  at room temperature over an extended time.

and complete conversion of **1**. The obvious blue shifts of the first two  $\nu_{\text{CO}}$  bands by 60 and 75  $\text{cm}^{-1}$  indicate the formation of the one-electron oxidized product  $[1]^+$ , and the broad low-intensity band at 1901  $\text{cm}^{-1}$  is typical of a semibridging CO ligand as reported for other  $\text{Fe}^{\text{II}}\text{Fe}^{\text{I}}$  models.<sup>19–22</sup> Similarly, the first two  $\nu_{\text{CO}}$  absorptions of **2** and **3** were blue-shifted rapidly by 57–73  $\text{cm}^{-1}$  as 1 equiv. of  $\text{FcBAR}_4^{\text{F}}$  was added to the solution (Fig. 5b, c and Table 1), indicating the formation of  $[2]^+$  and  $[3]^+$ , respectively.

Fig. 5d–f show that the *in situ* generated  $[1]^+$  in  $\text{CH}_2\text{Cl}_2$  is more stable than  $[2]^+$  and  $[3]^+$ , but it still slowly decomposed when standing in solution at room temperature under  $\text{N}_2$  for several hours. The intensity of the  $\nu_{\text{CO}}$  bands of  $[2]^+$  gradually dropped and almost disappeared after the solution of  $[2]^+$  stood for 2 h (Fig. 5e), accompanied by the appearance of two  $\nu_{\text{CO}}$  bands at 1915 and 1992  $\text{cm}^{-1}$ . As these two new  $\nu_{\text{CO}}$  bands did not emerge synchronously, they should be attributed to two decomposed products. By removal of the solvent from the resulting solution and flash column chromatography, one of the decomposed products of  $[2]^+$  was isolated as a black crystalline solid. The MS, IR,  $^1\text{H}$  and  $^{31}\text{P}\{^1\text{H}\}$  NMR spectra revealed that the dinuclear complex  $[2]^+$  has split to a mononuclear complex by losing the  $\text{Fe}(\text{CO})_3$  moiety. Similar disruption of the  $\text{Fe}_2\text{S}_2$  core was found during the ligand substitution reaction of all-CO diiron complexes bearing a bdt or its derivative bridge.<sup>35</sup> The strong rigidity of the bdt bridge makes this type of diiron dithiolate complex less stable than those bearing flexible alkylene bridges. The crystallographic analysis further confirmed that the isolated decomposed complex is a coordinately unsaturated  $\text{Fe}^{\text{II}}$  complex,  $[\text{Fe}(\text{CO})(\kappa^2\text{-bdtMe})(\kappa^2\text{-PNP})]$  (**2'**, Fig. S1†), which features a square pyramidal configuration with the CO at the pyramid apex. Analogous complexes  $[\text{Fe}(\text{CO})(\kappa^2\text{-bdt})\{\kappa^2\text{-(Ph}_2\text{PCH}_2)_2\text{N(R)}\}]$  (R =  $\text{CH}_2\text{CH}(\text{OCH}_2\text{CH}_3)_2$ ,  $\text{CH}_2\text{COONa}$ ) were prepared by the one-pot reaction of  $\text{FeCl}_2$ ,

$\text{bdtH}_2$ , CO, and diphosphine ligand in MeOH in the presence of triethylamine, and used as catalysts for hydrogen evolution reaction (HER).<sup>36,37</sup> To attribute the two  $\nu_{\text{CO}}$  absorptions in the final IR spectrum of Fig. 5e, we studied the oxidation reaction of **2'** by using an *in situ* IR spectroscopic technique. The  $\nu_{\text{CO}}$  absorption of **2'** at 1915  $\text{cm}^{-1}$  completely disappeared within 3 min upon addition of 1 equiv. of  $\text{FcBAR}_4^{\text{F}}$  (Fig. S2†). In the meantime, a  $\nu_{\text{CO}}$  band emerged at 1992  $\text{cm}^{-1}$ , suggesting that the iron center of **2'** is oxidized from  $\text{Fe}^{\text{II}}$  to  $\text{Fe}^{\text{III}}$  (**2''**). On the basis of these observations, we assume that the initially generated decomposed product of  $[2]^+$  is an  $\text{Fe}^{\text{II}}$  mononuclear complex (**2'**), which is oxidized *in situ* to a  $\text{Fe}^{\text{III}}$  complex by  $\text{Fc}^+$  in solution.

In comparison, the  $\nu_{\text{CO}}$  absorptions of  $[3]^+$  totally vanished after the solution of  $[3]^+$  stood under  $\text{N}_2$  for about 10 min, and more than five low-intensity bands were observed in the region of 2105–1990  $\text{cm}^{-1}$  (Fig. 5f). The quick decomposition of  $[3]^+$  in solution does not allow for further study of  $[3]^+$  on  $\text{H}_2$  activation. We notice that the analogous complex,  $[\text{Fe}_2(\mu\text{-adtBn})(\text{CO})_4(\kappa^2\text{-dppv})]^+$ , was also found to be unstable under identical conditions and the reason for the instability of this mixed-valence complex was assumed to be disproportionation caused by amine binding.<sup>25</sup> Altogether, the stability of this series of mixed-valence diiron complexes is in the order of  $[4]^+ > [1]^+ > [2]^+ \gg [3]^+$ . The stability of the  $\text{Fe}^{\text{II}}\text{Fe}^{\text{I}}$  intermediate is one of the key factors that determine the performance of  $\text{H}_{\text{ox}}$  models in the  $\text{H}_2$  activation due to the limit of the binding rate of  $\text{H}_2$  to the open coordination site at the rotated iron of the  $\text{Fe}^{\text{II}}\text{Fe}^{\text{I}}$  core.

#### Activation of $\text{H}_2$ by $[1]^+$ in the presence of $\text{Fc}^+$

The reaction of  $[1]^+$  with 1 atm  $\text{H}_2$  in the presence of  $\text{FcBAR}_4^{\text{F}}$  in  $\text{CH}_2\text{Cl}_2$  at 25 °C was studied by *in situ* IR spectroscopy. Two extra equiv. of  $\text{FcBAR}_4^{\text{F}}$  were added to the  $\text{CH}_2\text{Cl}_2$  solution

containing the *in situ* generated  $[1]^+$ , and  $H_2$  was bubbled into the solution for 10 min. As expected, the three  $\nu_{CO}$  absorptions of  $[1]^+$  gradually decreased and eventually disappeared within a period of 2 h (Fig. S3<sup>†</sup>). In contrast, it took 4 h for the complete conversion of  $[4]^+$  under the same conditions,<sup>30</sup> indicating that  $[1]^+$  is more active than  $[4]^+$  for  $H_2$  activation, but it is less stable than  $[4]^+$ . After the reaction of  $[1]^+$  with  $H_2/Fc^+$  for 2 h, the resulting solution displayed four  $\nu_{CO}$  bands at 2107, 2051, 2003, and 1972  $cm^{-1}$  in the IR spectrum (Fig. 6a). A comparison of these  $\nu_{CO}$  absorptions with those observed for the cationic products formed by the direct protonation of **1** in the presence of TfOH (Fig. 6b and S4<sup>†</sup>) reveals that the resulting solution contains a mixture of  $[1(H_\mu)(H_N)]^{2+}$ ,  $[1(H_\mu)]^+$ , and  $[1(H_N)]^+$ , as well as the decomposed species of  $[1]^+$ . Upon addition of an excess of  $P(o\text{-tol})_3$  to the resulting solution, the neutral complex **1** was recovered partially as evidenced by

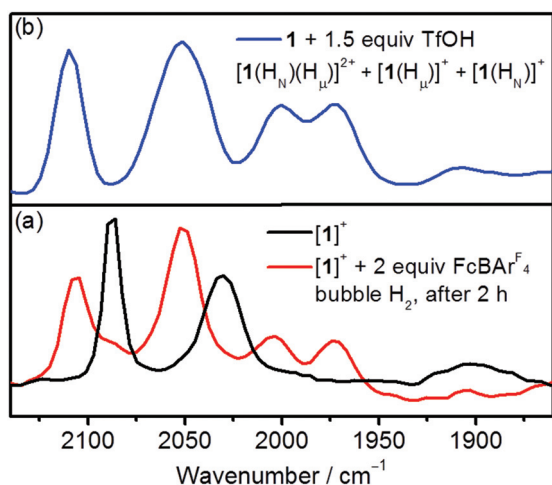
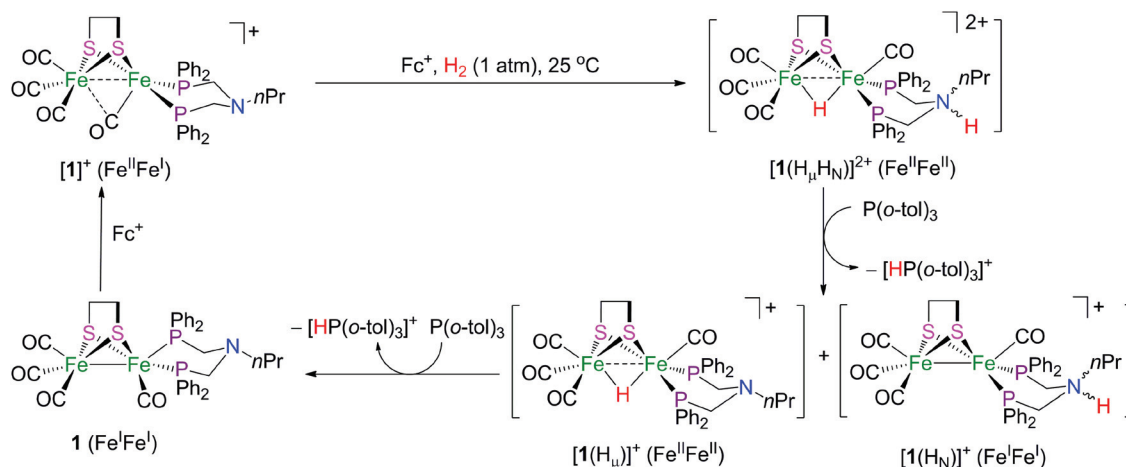


**Fig. 6** Selected region of the *in situ* IR spectra (a) for the  $\nu_{CO}$  absorptions of  $[1]^+$  and the resulting solution from the reaction of  $[1]^+$  and  $FcBARF_4$  in  $CH_2Cl_2$  under 1 atm  $H_2$  at 25 °C for 2 h. (b) The  $\nu_{CO}$  absorptions of the cationic products formed by direct protonation of **1** in the presence of 1.5 equiv. of TfOH.

*in situ* IR spectra (Fig. S5<sup>†</sup>), indicating that part of **1** was decomposed during the reaction. The  $^{31}P\{^1H\}$  NMR spectrum of the resulting solution does not show discernable signals, possibly due to the disturbance of the decomposed paramagnetic iron species existing in the solution.

The reaction of  $[2]^+$  with 1 atm  $H_2$  in the presence of 2 equiv. of  $FcBARF_4$  was also studied. The *in situ* IR spectra (Fig. S6<sup>†</sup>) show that  $[2]^+$  decomposes to the mononuclear complex regardless of whether or not the reaction was carried out under  $H_2$  or  $N_2$ , and the decomposed  $Fe^{II}$  complex was oxidized to the  $Fe^{III}$  complex ( $2''$ ) due to the existence of an excess of  $Fc^+$  in the solution.  $[2]^+$  cannot activate  $H_2$  in the presence of  $Fc^+$  under mild conditions.

Moreover, the catalytic activation of  $H_2$  by **1** was studied. First,  $FcPF_6$  was used for the oxidation of **1** to  $[1]^+$ , and the following  $H_2$  oxidation reaction was carried out in the presence of 20 equiv. of  $FcBARF_4$  and 20 equiv. of  $P(o\text{-tol})_3$  under 1 atm  $H_2$  at 25 °C. The supplemental  $FcBARF_4$  and  $P(o\text{-tol})_3$  are required to act as an electron acceptor and a proton trapper, respectively, in the activation of  $H_2$  by  $H_{ox}$  models. After 8 h of reaction, the conversion of  $P(o\text{-tol})_3$  to  $[HP(o\text{-tol})_3]^+$  was detected by  $^{31}P\{^1H\}$  NMR spectroscopy (Fig. S7<sup>†</sup>), which gave a turnover of  $2.3(\pm 0.1)$  moles of  $H_2$  consumed per mol of **1**. We found that the bulky counter ion  $BARF_4^-$  can stabilize the  $Fe^{II}Fe^I$  intermediate  $[1]^+$ . If  $FcBARF_4$  was used for the oxidation of **1**, the following  $H_2$  oxidation reaction by  $FcBARF_4$  is apparently slower than using  $FcPF_6$  for the oxidation of **1** in the first step. It might be possible that the F atoms of  $PF_6^-$  could help to shuttle protons and thereby to facilitate the heterolytic cleavage of  $H_2$ .<sup>38,39</sup> In a reverse case, if  $FcPF_6$  was used for both the oxidation of **1** and the following  $H_2$  oxidation reaction, more decomposed species of **1** was detected by *in situ* IR spectroscopy during the  $H_2$  oxidation process. To the best of our knowledge, among the  $[FeFe]-H_2ase$  models so far reported, only two diiron complexes have been reported to be catalytically active for the  $H_2$  oxidation reaction under mild conditions. By comparison, the turnover numbers for  $H_2$  activation are 2 in 5 h for  $[(\mu\text{-adtBn})\{Fe(CO)_2(FcP^*)\}\{Fe(CO)(\kappa^2-$



**Scheme 1** Proposed pathway for  $H_2$  activation by  $[1]^+$  and  $Fc^+$  in the presence of  $P(o\text{-tol})_3$ .

dppv)] and 6.2 in 10 h for **4** under similar conditions.<sup>26,30</sup> The control experiments showed that no signal was detected at  $\delta$  -13.57 for  $[\text{HP}(o\text{-tol})_3]^+$  in the  $^{31}\text{P}\{^1\text{H}\}$  NMR spectra when the reaction was carried out in the absence of **1** or  $\text{Fc}^+$  under otherwise identical conditions.

To have some insight into the mechanism of the  $\text{H}_2$  activation reaction, we carried out the following control reactions. First, neither  $[\mathbf{1}]^+$  nor  $\text{Fc}^+$  reacted with 1 atm  $\text{H}_2$  under mild conditions. Second,  $[\mathbf{1}]^+$  could not be oxidized by  $\text{FcBAR}_4^{\text{F}}$  as the second oxidation potential of **1** is more positive than the reduction potential of  $\text{Fc}^+$  (Fig. S8†). In view of these observations, the heterolytic cleavage of the H–H bond should be a process involving  $[\mathbf{1}]^+$ ,  $\text{Fc}^+$ , and  $\text{H}_2$ . The details of this synergistic process are currently not clear. Just as  $[\mathbf{4}]^+$  and other reported  $[\text{Fe}_2\{\mu\text{-S}\}_2\text{R}\{\text{CO}\}_4(\text{P}^{\wedge}\text{P})]^+$  models,<sup>20,21,30</sup>  $[\mathbf{1}]^+$  with an open apical site at the iron center of the rotated  $\text{Fe}(\text{CO})(\text{PNP})$  unit could allow a coordinative interaction of this iron center with a molecule of  $\text{H}_2$ . The  $\text{H}_2$  activation is possibly through the similar pathway proposed for other  $\text{H}_{\text{ox}}$  models as shown in Scheme 1.<sup>29,30,40</sup> Coordination of  $\text{H}_2$  to the open apical site of the rotated Fe unit is accompanied by or immediately followed by the oxidation of the intermediate by  $\text{Fc}^+$ ; the H–H bond of the coordinating  $\text{H}_2$  molecule is then heterolytically cleaved with the assistance of the internal amine to form an intermediate  $[\mathbf{1}(\text{H}_\text{N}\text{H}_\mu)]^{2+}$ , which readily converts to  $[\mathbf{1}(\text{H}_\mu)]^+$  and  $[\mathbf{1}(\text{H}_\text{N})]^+$  via partial deprotonation by  $\text{P}(o\text{-tol})_3$  and finally back to **1** by further deprotonation to fulfill a complete catalytic cycle.

## Conclusions

In summary, three new  $[\text{FeFe}]\text{-H}_2\text{ase}$  models (**1–3**) with the same *N*-containing diphosphine ligand but with different S-to-S bridges were prepared, and their molecular structures were determined by single-crystal X-ray diffraction. Electrochemical studies show that the electronic properties and rigidity of S-to-S bridges in these complexes have a limited effect on the oxidation potential for the  $\text{Fe}^{\text{I}}\text{Fe}^{\text{I}}/\text{Fe}^{\text{II}}\text{Fe}^{\text{I}}$  couple but have a considerable influence on the potential for the  $\text{Fe}^{\text{II}}\text{Fe}^{\text{I}}/\text{Fe}^{\text{II}}\text{Fe}^{\text{II}}$  oxidation, while the potential for the  $\text{Fe}^{\text{II}}\text{Fe}^{\text{I}}/\text{Fe}^{\text{II}}\text{Fe}^{\text{II}}$  oxidation is less susceptible to the length of the S-to-S linker compared to the first oxidation potential. As a consequence, the S-to-S bridge apparently influences the  $\Delta E^{\text{ox}}$  ( $|E_{\text{p}}^{\text{ox}2} - E_{\text{p}}^{\text{ox}1}|$ ) value. To design effective  $\text{H}_{\text{ox}}$  models for  $\text{H}_2$  activation, this value should be large enough to ensure that the second oxidation process does not overlap with the first one. When the further oxidation reaction of the mixed-valence complex is suppressed, the coordination of the  $\text{H}_2$  molecule to the Fe center and the oxidation of the  $\text{H}_{\text{ox}}$  model could occur in a synergetic manner. Accordingly, complex **1** with a large  $\Delta E^{\text{ox}}$  value can be cleanly oxidized by  $\text{Fc}^+$  to give a metastable mixed-valence complex  $[\mathbf{1}]^+$ , which displayed catalytic activity for  $\text{H}_2$  oxidation in the presence of an excess oxidant and a proton trapper. Although the two single-electron oxidation events of **2** are well separated,  $[\mathbf{2}]^+$  cannot activate  $\text{H}_2$  in the presence of  $\text{Fc}^+$ ; it decomposed

to the mononuclear complex **2'** to release the ring strain caused by the rigid bdtMe bridge in the diiron complex. In contrast to **1** and **2**, complex **3** with an adtBn bridge has a small  $\Delta E^{\text{ox}}$  value; the further oxidation of the *in situ* generated  $[\mathbf{3}]^+$  leads to its rapid decomposition. Introduction of an internal amine base into the S-to-S bridge of the  $\text{H}_{\text{ox}}$  model bearing a PNP ligand does not result in a concerted effect of these two pendant bases in  $\text{H}_2$  activation, but considerably speeds up the decomposition of the  $\text{H}_{\text{ox}}$  model. The results of the present work clearly show that changing the S-to-S bridge can effectively tune the oxidation potentials and the stability of  $\text{H}_{\text{ox}}$  models, and consequently bring about a great effect on the performance of the mixed-valence diiron complex for  $\text{H}_2$  activation.

## Experimental section

### Materials and instruments

All reactions and operations related to organometallic complexes were carried out under dry, oxygen-free  $\text{N}_2$  with standard Schlenk techniques. The solvents were dried and distilled prior to use according to the standard methods. The reagents  $\text{FcPF}_6$  and  $\text{P}(o\text{-tol})_3$  were purchased from Aldrich, and  $\text{LiB}(\text{H})\text{Et}_3$  from Aladdin. The other commercially available chemicals such as ethane-1,2-dithiol, toluene-3,4-dithiol, benzylamine, *n*-propylamine, paraformaldehyde,  $\text{Fe}(\text{CO})_5$ , and  $\text{Cp}_2\text{Fe}$  were purchased from local companies. All reagents were used as received. Compounds  $\text{PNP}$ ,<sup>41</sup>  $[(\mu\text{-edt})\text{Fe}_2(\text{CO})_6]$ ,<sup>42</sup>  $[(\mu\text{-bdtMe})\text{Fe}_2(\text{CO})_6]$ ,<sup>43</sup>  $[(\mu\text{-adtBn})\text{Fe}_2(\text{CO})_6]$ ,<sup>44</sup> and  $\text{FcBAR}_4^{\text{F}}$ <sup>45,46</sup> were synthesized according to the literature procedures.

Infrared spectra were recorded with a JASCO FT/IR 430 spectrophotometer. *In situ* IR spectra were recorded on a Mettler-Toledo-IR™ 15 System equipped with an MCT detector and a Dsub AgX SiComp™ *in situ* probe.  $^1\text{H}$  and  $^{31}\text{P}$  NMR spectra were recorded with a Bruker Avance III 500 spectrometer. Mass spectra were recorded on a LTQ Orbitrap XL instrument.

### Synthesis of 1–3

A toluene solution (20 mL) containing  $[(\mu\text{-edt})\text{Fe}_2(\text{CO})_6]$  (0.35 g, 1.0 mmol) and ligand PNP (0.46 g, 1.0 mmol) was refluxed for 3 h and the color of the solution turned from red to dark green. After the reaction, the solvent was removed under reduced pressure. The residue was washed several times with hexane/ $\text{CH}_2\text{Cl}_2$  (5 : 1, v/v) and then purified by chromatography on a silica gel column with hexane/ $\text{CH}_2\text{Cl}_2$  (3 : 1, v/v) as the eluent. A red powder was obtained from the collected orange band after removal of the solvent. Yield of **1**: 0.58 g (75%). Single crystals suitable for X-ray analysis were obtained by recrystallization of the product from hexane/ $\text{CH}_2\text{Cl}_2$  solution under  $\text{N}_2$  at room temperature.  $^1\text{H}$  NMR (500 MHz,  $\text{CDCl}_3$ ):  $\delta$  7.63–7.23 (m, 20H, 4Ph), 3.71, 3.17 (2br s, 4H,  $\text{PCH}_2\text{NCH}_2\text{P}$ ), 2.44 (br s, 2H,  $\text{NCH}_2\text{C}$ ), 1.82, 1.67 (2br s, 4H,  $\text{SCH}_2\text{CH}_2\text{S}$ ), 1.26 (m, 2H,  $\text{NCH}_2\text{CH}_2$ ), 0.58 (br s, 3H,  $\text{CH}_2\text{CH}_3$ ).  $^{31}\text{P}\{^1\text{H}\}$  NMR

(204 MHz, CDCl<sub>3</sub>):  $\delta$  53.58 (s). IR (CH<sub>2</sub>Cl<sub>2</sub>):  $\nu_{\text{CO}}$  2028, 1956, 1900 cm<sup>-1</sup>. ESI-HRMS:  $m/z$  = 772.0260 (Calcd for [M + H]<sup>+</sup>:  $m/z$  = 772.0260).

Complexes **2** and **3** were prepared as dark green crystalline solids with an essentially identical procedure to that used for the preparation of **1**. Yield of **2**: 0.51 g (61%). <sup>1</sup>H NMR (500 MHz, CDCl<sub>3</sub>):  $\delta$  7.52–5.97 (m, 23H, 4Ph and C<sub>6</sub>H<sub>3</sub>), 3.85, 3.32 (2br s, 4H, PCH<sub>2</sub>NCH<sub>2</sub>P), 2.54 (t, 2H, NCH<sub>2</sub>C,  $J$  = 7.3 Hz), 1.81 (s, 3H, C<sub>6</sub>H<sub>3</sub>CH<sub>3</sub>), 1.36 (m, 2H NCH<sub>2</sub>CH<sub>2</sub>), 0.63 (t, 3H, CH<sub>2</sub>CH<sub>3</sub>,  $J$  = 7.3 Hz). <sup>31</sup>P{<sup>1</sup>H} NMR (204 MHz, CDCl<sub>3</sub>):  $\delta$  53.88. IR (CH<sub>2</sub>Cl<sub>2</sub>):  $\nu_{\text{CO}}$  2033, 1963, 1901 cm<sup>-1</sup>. ESI-HRMS:  $m/z$  = 834.0387 (Calcd for [M + H]<sup>+</sup>:  $m/z$  = 834.0416).

Yield of **3**: 0.44 g (51%). <sup>1</sup>H NMR (500 MHz, CDCl<sub>3</sub>):  $\delta$  7.56–6.59 (m, 25H, 5Ph), 3.77, 3.16 (2br s, 4H, PCH<sub>2</sub>NCH<sub>2</sub>P), 2.93 (s, 2H, NCH<sub>2</sub>Ph), 2.74 (d, 2H, SCH<sub>2</sub>N,  $J$  = 10.0 Hz), 2.44 (br s, 2H, NCH<sub>2</sub>C), 2.33 (d, 2H, NCH<sub>2</sub>S,  $J$  = 10.5 Hz), 1.26 (m, 2H, NCH<sub>2</sub>CH<sub>2</sub>), 0.57 (br s, 3H, CH<sub>2</sub>CH<sub>3</sub>). <sup>31</sup>P{<sup>1</sup>H} NMR (204 MHz, CDCl<sub>3</sub>):  $\delta$  53.42. IR (CH<sub>2</sub>Cl<sub>2</sub>):  $\nu_{\text{CO}}$  2026, 1955, 1901 cm<sup>-1</sup>. ESI-HRMS:  $m/z$  = 877.0823 (Calcd for [M + H]<sup>+</sup>:  $m/z$  = 877.0838).

### Decomposition of [2]<sup>+</sup> to 2'

The complex [2]<sup>+</sup> was freshly formed from the reaction of **2** (0.50 g, 0.6 mmol) and FcPF<sub>6</sub> (0.20 g, 0.6 mmol) in CH<sub>2</sub>Cl<sub>2</sub> under Ar. The solution was stirred for 6 h at 25 °C. After the reaction, the solvent was removed under reduced pressure and the residue was purified by chromatography on a silica gel column with hexane/CH<sub>2</sub>Cl<sub>2</sub> (1:3, v/v) as the eluent. A black powder was obtained from the collected black band after removal of the solvent. Yield of 2': 0.24 g (58%). Single crystals suitable for X-ray analysis were obtained by recrystallization of the product from hexane/CH<sub>2</sub>Cl<sub>2</sub> solution under N<sub>2</sub> at room temperature. <sup>1</sup>H NMR (500 MHz, CDCl<sub>3</sub>):  $\delta$  7.93–6.91 (m, 23H, 4Ph and C<sub>6</sub>H<sub>3</sub>), 3.97 (t, 2H, PCH<sub>2</sub>N,  $J$  = 10.1 Hz), 3.27 (t, 2H, PCH<sub>2</sub>N,  $J$  = 10.4 Hz), 2.66 (t, 2H, NCH<sub>2</sub>C,  $J$  = 10.0 Hz), 2.34 (s, 3H, C<sub>6</sub>H<sub>3</sub>CH<sub>3</sub>), 1.57 (m, 2H NCH<sub>2</sub>CH<sub>2</sub>), 0.88 (m, 3H, CH<sub>2</sub>CH<sub>2</sub>CH<sub>3</sub>). <sup>31</sup>P{<sup>1</sup>H} NMR (204 MHz, CDCl<sub>3</sub>):  $\delta$  50.84 (s). IR (CH<sub>2</sub>Cl<sub>2</sub>):  $\nu_{\text{CO}}$  1915 cm<sup>-1</sup>. ESI-HRMS:  $m/z$  = 694.1181 (Calcd for [M + H]<sup>+</sup>:  $m/z$  = 694.1219). The same product 2' was isolated from the resulting solution of the reaction of [2]<sup>+</sup> and excess FcBAR<sup>F</sup><sub>4</sub> under 1 atm H<sub>2</sub> at 25 °C for 8 h.

### Activation of H<sub>2</sub> by [1]<sup>+</sup> in the presence of FcBAR<sup>F</sup><sub>4</sub>

The oxidant FcPF<sub>6</sub> (13.3 mg, 0.04 mmol) was added to a CH<sub>2</sub>Cl<sub>2</sub> solution (5 mL) of **1** (30.8 mg, 0.04 mmol) under Ar. The solution was stirred for 20 min at 25 °C and the reaction was monitored by *in situ* IR spectroscopy. After complex **1** was completely oxidized to [1]<sup>+</sup> according to IR spectra, FcBAR<sup>F</sup><sub>4</sub> (83.6 mg, 0.08 mmol) was added to the resulting solution and H<sub>2</sub> gas was bubbled through the solution for 10 min. The solution was stirred under an atmosphere of H<sub>2</sub> (1.0 atm) at 25 °C. After the  $\nu_{\text{CO}}$  bands of [1]<sup>+</sup> disappeared (about 2 h), P(*o*-tol)<sub>3</sub> (24.3 mg, 0.08 mmol) was added to the resulting solution to recover the starting complex **1**.

### Catalytic oxidation of H<sub>2</sub> by [1]<sup>+</sup> in the presence of FcBAR<sup>F</sup><sub>4</sub> and P(*o*-tol)<sub>3</sub>

The oxidant FcPF<sub>6</sub> (3.3 mg, 0.01 mmol) was added to a CH<sub>2</sub>Cl<sub>2</sub> solution (10 mL) of **1** (7.8 mg, 0.01 mmol) under N<sub>2</sub>. The mixture was stirred for 10 min at 25 °C. Next, FcBAR<sup>F</sup><sub>4</sub> (209 mg, 0.2 mmol) and P(*o*-tol)<sub>3</sub> (61 mg, 0.2 mmol) were added to the solution and H<sub>2</sub> gas was bubbled through the solution for 10 min. The solution was stirred for 8 h at 25 °C under an atmosphere of H<sub>2</sub> (1.0 atm). The resulting solution was detected by quantitative <sup>31</sup>P{<sup>1</sup>H} NMR spectroscopy and a turnover of 2.3(±0.1) moles of H<sub>2</sub> per mole of **1** was calculated on the basis of the conversion of P(*o*-tol)<sub>3</sub> to [HP(*o*-tol)<sub>3</sub>]<sup>+</sup>.

Quantitative <sup>31</sup>P{<sup>1</sup>H} NMR spectra of the resulting solution containing P(*o*-tol)<sub>3</sub> and [HP(*o*-tol)<sub>3</sub>]<sup>+</sup> were recorded using the inverse gate proton decoupling technique for the suppression of the nuclear Overhauser effect on a Bruker Avance III 500 with the following instrument settings: temperature = 298 K, spectrometer frequency for <sup>31</sup>P = 203.720 MHz, sweep width = 81 521.742 Hz, 32 768 data points, 90° excitation pulse.

The TON of H<sub>2</sub> uptake was calculated by the following equation:

$$\text{TON} = A_1 \times n_o / [2(A_1 + A_2) \times n_{\text{cat}}] \quad (\text{mol H}_2 \text{ per mol catalyst})$$

$A_1$  = the integrated area for the <sup>31</sup>P{<sup>1</sup>H} NMR signal of [HP(*o*-tol)<sub>3</sub>]<sup>+</sup>,  $A_2$  = the integrated area for the <sup>31</sup>P{<sup>1</sup>H} NMR signal of P(*o*-tol)<sub>3</sub>,  $n_o$  = the total mol of P(*o*-tol)<sub>3</sub> added to the solution, and  $n_{\text{cat}}$  = total mol of the catalyst in solution.

### Electrochemical studies

Cyclic voltammograms were obtained in a three-electrode cell under Ar using CHI 630D electrochemical work station. The working electrode was a glassy carbon disc (diameter 3 mm) polished with 3 and 1 μm diamond pastes and sonicated in ion-free water for 15 min prior to use. The reference electrode was a non-aqueous Ag<sup>+</sup>/Ag (0.01 M AgNO<sub>3</sub> in CH<sub>3</sub>CN) electrode and the counter electrode was platinum wire. Methylene chloride was freshly distilled over P<sub>2</sub>O<sub>5</sub> before being used for electrochemical studies. A solution of 0.1 M *n*Bu<sub>4</sub>NPF<sub>6</sub> (Fluka, electrochemical grade) in CH<sub>2</sub>Cl<sub>2</sub> was used as a supporting electrolyte and was degassed by bubbling with dry argon for 10 min before measurement. The ferricinium/ferrocene (Fc<sup>+</sup>/Fc) couple was used as an internal reference and all potentials given in this work are referred to the Fc<sup>+0</sup> potential.

### Determination of the structures of 1–3

The single crystal X-ray diffraction data were collected with a Bruker Smart Apex II CCD diffractometer with graphite-monochromated Mo-K<sub>α</sub> radiation ( $\lambda$  = 0.071073 Å) at 296 K using the  $\omega$ -2 $\theta$  scan mode. Data processing was accomplished with the SAINT processing program.<sup>47</sup> Intensity data were corrected for absorption by using the SADABS program.<sup>48</sup> All structures were solved by direct methods and refined on  $F^2$  against full-matrix least-squares methods by using the SHELXTL 97 program package.<sup>49</sup> All non-hydrogen atoms were refined anisotropically. Hydrogen atoms were located by geometrical calculation.

Details of crystallographic data and processing parameters are summarized in Table S2.†

## Acknowledgements

We are grateful to the National Natural Science Foundation of China (Grant No. 21373040, 21673028, 21120102036 and 21361130020), the Basic Research Program of China (No. 2014CB239402), the Ph.D. Program Foundation of Ministry of Education of China (No. 20130041110024), the Swedish Energy Agency, the Swedish Research Council and the K & A Wallenberg Foundation for the financial support of this work.

## Notes and references

- M. W. W. Adams and E. I. Stiefel, *Science*, 1998, **282**, 1842–1843.
- R. Cammack, *Nature*, 1999, **397**, 214–215.
- Y. Nicolet, C. Cavazza and J. C. Fontecilla-Camps, *J. Inorg. Biochem.*, 2002, **91**, 1–8.
- D. J. Evans and C. J. Pickett, *Chem. Soc. Rev.*, 2003, **32**, 268–275.
- Y. Nicolet, C. Piras and P. Legrand, *Structure*, 1999, **7**, 13–23.
- J. W. Peters, N. L. William, J. L. Brian and C. S. Lance, *Science*, 1998, **282**, 1853–1858.
- A. Adamska, A. Silakov, C. Lambertz, O. Ruediger, T. Happe, E. Reijerse and W. Lubitz, *Angew. Chem., Int. Ed.*, 2012, **51**, 11458–11462.
- Z. Chen, B. J. Lemon, S. Huang, D. J. Swartz, J. W. Peters and K. A. Bagley, *Biochemistry*, 2002, **41**, 2036–2043.
- Z.-P. Liu and P. Hu, *J. Am. Chem. Soc.*, 2002, **124**, 5175–5182.
- J.-F. Capon, F. Gloaguen, F. Y. Petillon, P. Schollhammer and J. Talarmin, *Coord. Chem. Rev.*, 2009, **253**, 1476–1494.
- I. P. Georgakaki, L. M. Thomson, E. J. Lyon, M. B. Hall and M. Y. Darensbourg, *Coord. Chem. Rev.*, 2003, **238–239**, 255–266.
- J.-F. Capon, F. Gloaguen, P. Schollhammer and J. Talarmin, *Coord. Chem. Rev.*, 2005, **249**, 1664–1676.
- X. Liu, S. K. Ibrahim, C. Tard and C. J. Pickett, *Coord. Chem. Rev.*, 2005, **249**, 1641–1652.
- G. A. N. Felton, C. A. Mebi, B. J. Petro, A. K. Vannucci, D. H. Evans, R. S. Glass and D. L. Lichtenberger, *J. Organomet. Chem.*, 2009, **694**, 2681–2699.
- C. Tard and C. J. Pickett, *Chem. Rev.*, 2009, **109**, 2245–2274.
- S. Tschierlei, S. Ott and R. Lomoth, *Energy Environ. Sci.*, 2011, **4**, 2340–2352.
- N. Wang, M. Wang, L. Chen and L. Sun, *Dalton Trans.*, 2013, **42**, 12059–12071.
- M. Razavet, S. J. Borg, S. J. George, S. P. Best, S. A. Fairhurst and C. J. Pickett, *Chem. Commun.*, 2002, 700–701.
- T. Liu and M. Y. Darensbourg, *J. Am. Chem. Soc.*, 2007, **129**, 7008–7009.
- A. K. Justice, T. B. Rauchfuss and S. R. Wilson, *Angew. Chem., Int. Ed.*, 2007, **46**, 6152–6154.
- A. K. Justice, L. D. Gioia, M. J. Nilges, T. B. Rauchfuss, S. R. Wilson and G. Zampella, *Inorg. Chem.*, 2008, **47**, 7405–7414.
- M. L. Singleton, N. Bhuvanesh, J. H. Reibenspies and M. Y. Darensbourg, *Angew. Chem., Int. Ed.*, 2008, **47**, 9492–9495.
- A. K. Justice, M. J. Nilges, T. B. Rauchfuss, S. R. Wilson, L. De Gioia and G. Zampella, *J. Am. Chem. Soc.*, 2008, **130**, 5293–5301.
- M. T. Olsen, B. E. Barton and T. B. Rauchfuss, *Inorg. Chem.*, 2009, **48**, 7507–7509.
- J. M. Camara and T. B. Rauchfuss, *J. Am. Chem. Soc.*, 2011, **133**, 8098–8101.
- J. M. Camara and T. B. Rauchfuss, *Nat. Chem.*, 2012, **4**, 26–30.
- N. Wang, M. Wang, T. Zhang, P. Li, J. Liu and L. Sun, *Chem. Commun.*, 2008, 5800–5802.
- N. Wang, M. Wang, L. Liu, K. Jin, L. Chen and L. Sun, *Inorg. Chem.*, 2009, **48**, 11551–11558.
- Y. Wang and M. S. G. Ahlquis, *Dalton Trans.*, 2013, **42**, 7816–7822.
- N. Wang, M. Wang, Y. Wang, D. Zheng, H. Han, M. S. G. Ahlquist and L. Sun, *J. Am. Chem. Soc.*, 2013, **135**, 13688–13691.
- X. Zhao, I. P. Georgakaki, M. L. Miller, R. Mejia-Rodriguez, C.-Y. Chiang and M. Y. Darensbourg, *Inorg. Chem.*, 2002, **41**, 3917–3928.
- F. Gloaguen, J. D. Lawrence, T. B. Rauchfuss, M. Benard and M.-M. Rohmer, *Inorg. Chem.*, 2002, **41**, 6573–6582.
- D. Morvan, J.-F. Capon, F. Gloaguen, A. L. Goff, M. Marchivie, F. Michaud, P. Schollhammer, J. Talarmin and J.-J. Yaoquanc, *Organometallics*, 2007, **26**, 2042–2052.
- M. T. Olsen, T. B. Rauchfuss and S. R. Wilson, *J. Am. Chem. Soc.*, 2010, **132**, 17733–17740.
- L. Schwartz, P. S. Singh, L. Eriksson, R. Lomoth and S. Ott, *C. R. Chim.*, 2008, **11**, 875–889.
- M. Beyler, S. Ezzaher, M. Karnahl, M.-P. Santoni, R. Lomoth and S. Ott, *Chem. Commun.*, 2011, **47**, 11662–11664.
- J. M. Gardner, M. Beyler, M. Karnahl, S. Tschierlei, S. Ott and L. Hammarström, *J. Am. Chem. Soc.*, 2012, **134**, 19322–19325.
- Z. M. Heiden and T. B. Rauchfuss, *J. Am. Chem. Soc.*, 2009, **131**, 3593–3600.
- A. Macchioni, *Chem. Rev.*, 2005, **105**, 2039–2074.
- H.-J. Fan and M. B. Hall, *J. Am. Chem. Soc.*, 2001, **123**, 3828–3829.
- A. L. Balch, M. M. Olmstead and S. P. Rowley, *Inorg. Chim. Acta*, 1990, **168**, 255–264.
- F. Gloaguen, J. D. Lawrence, M. Schmidt, S. R. Wilson and T. B. Rauchfuss, *J. Am. Chem. Soc.*, 2001, **123**, 12518–12527.
- A. Winter, L. Zsolnai and G. Huttner, *Z. Naturforsch., B: Anorg. Chem. Org. Chem.*, 1982, **37**, 1430–1436.

- 44 J. D. Lawrence, H. Li and T. B. Rauchfuss, *Chem. Commun.*, 2001, 1482–1483.
- 45 M. Brookhart, B. Grant and A. F. Volpe Jr., *Organometallics*, 1992, **11**, 3920–3922.
- 46 J. L. Bras, H. Jiao, W. E. Meyer, F. Hampel and J. A. Gladysz, *J. Organomet. Chem.*, 2000, **616**, 54–66.
- 47 G. M. Sheldrick, *SHELXTL97 Program for the Refinement of Crystal Structure*, University of Göttingen, Germany, 1997.
- 48 *Software packages SMART and SAINT*, Siemens Energy & Automation Inc., Madison, Wisconsin, 1996.
- 49 G. M. Sheldrick, *SADABS, Absorption Correction Program*, University of Göttingen, Göttingen, Germany, 1996.